UC Irvine
UC Irvine Previously Published Works

Title
Chromophore detection by fluorescence spectroscopy in tissue-like phantoms

Permalink
https://escholarship.org/uc/item/5g26j5sp

Authors
Cerussi, Albert E
Fantini, Sergio
Maier, John S
et al.

Publication Date
1997-08-18

DOI
10.1117/12.280240

Copyright Information
This work is made available under the terms of a Creative Commons Attribution License, availalbe at https://creativecommons.org/licenses/by/4.0/

Peer reviewed

eScholarship.org Powered by the California Digital Library
University of California

Chromophore detection by fluorescence spectroscopy in tissue-like phantoms

A. E. Cerussi, S. Fantini, J. S. Maier, W. W. Mantulin, and E. Gratton

Laboratory for Fluorescence Dynamics, Department of Physics,
University of Illinois at Urbana-Champaign, Urbana, IL 61801-3080

ABSTRACT

In the near-infrared spectral region (700-900 nm) light penetrates a few centimeters into tissues and hemoglobin dominates the absorption. Consequently, *in vivo* near-infrared tissue absorption spectroscopy becomes difficult for endogenous compounds of biological interest other than hemoglobin. Exogenous chromophore detection by fluorescence spectroscopy has the potential to provide enhanced sensitivity and specificity for *in vivo* optical tissue spectroscopy, facilitating the study of many important metabolites in tissues other than hemoglobin. We have performed measurements of the *DC* fluorescence intensity generated by a fluorophore (rhodamine B) homogeneously dissolved inside a highly scattering tissue-simulating phantom (aqueous suspension of titanium-dioxide particles). The phantom was prepared with optical coefficients (absorption and reduced scattering) similar to those of tissue in the near-infrared; these coefficients were measured with a frequency-domain spectrometer. Measurable *DC* fluorescence intensity signals from 1 nM rhodamine concentrations inside the phantom are reported. Furthermore, we were able to resolve changes in rhodamine concentration on the order of 1% using the *DC* fluorescence intensity. This *DC* fluorescence sensitivity is characterized experimentally at two concentrations (55 and 360 nM) and over a range of source-detector separations. Other aspects of the sensitivity are discussed over a large range of concentrations using a fluorescence photon migration model.

Keywords: fluorescence spectroscopy, frequency-domain, fluorescence sensitivity, fluorescence photon migration, diffusion theory, tissue spectroscopy

1. INTRODUCTION

1.1 *IN VIVO* HEMOGLOBIN MONITORING VIA OPTICAL TISSUE SPECTROSCOPY

Near-infrared (near-IR) optical tissue spectroscopy provides the possibility for monitoring physiological processes such as hemoglobin saturation *in vivo*.[1] Photons in the near-IR window (700-900 nm) penetrate a few centimeters below the skin and probe the underlying tissue volume. Both oxygenated and de-oxygenated forms of hemoglobin are responsible for most of the absorption of light within this near-IR window.[2,3] The success of *in vivo* hemoglobin monitoring relies heavily upon favorable sensitivity to the concentration of hemoglobin in the tissue. Other

Downloaded From: http://proceedings.spiedigitallibrary.org/ on 08/29/2016 Terms of Use: http://spiedigitallibrary.org/ss/termsofuse.aspx

important substances in tissues, such as glucose and Ca^{++}, do not stand out from the rest of the tissue as detectable absorbers of near-IR light. Thus, many important endogenous substances in tissues are quite difficult to monitor with absorption spectroscopy in the near-IR region.

1.2 FLUORESCENCE SPECTROSCOPY OFFERS THE POTENTIAL OF ENHANCED SENSITIVITY

Favorable signal-to-noise ratios are a general strength of fluorescence spectroscopy. Exogenous fluorescent markers, known for their specificity, may be used to selectively selective bind to specific substances of critical biological importance. Highly specific binding fluorescent dyes have been used for many years in microscopy and in the study of biological macromolecules. Although the autofluorescence of tissues has been used for diagnosing tissue slices,[4] exogenous fluorophores can provide sensitive markers for specific physiological metabolites. The ability to monitor *in vivo* substances in tissues would be of great usefulness to the medical/physiological community. Various aspects of fluorescence spectroscopy, such as fluorescence spectra[5] and lifetime sensing,[6] have been considered for *in vivo* tissue diagnostics.

However, the application of fluorescence spectroscopy to tissues revolves around an understanding of how fluorescence originates and propagates inside the tissue. Several groups have adopted diffusion theory to describe the creation and propagation of fluorescence light inside highly scattering media such as tissues in steady-state,[7] time-resolved,[8] and frequency-domain[9–11] cases. Although this approach has been experimentally verified both qualitatively and quantitatively, its experimental limits remain an open question.

1.3 GOAL AND SCOPE OF THIS WORK

Although fluorescence spectroscopy offers greater sensitivity than absorption spectroscopy in standard low-concentration non-scattering solutions, we would like to know if this is still true in the multiple-scattering regime. We sought to establish if nM concentrations of uniformly distributed fluorophores are realistically detectable inside multiple-scattering media. The quantification of the fluorescence sensitivity remains unanswered. For example, how well can we resolve between two similar, but not equal, fluorophore concentrations? Within what concentration ranges does fluorescence spectroscopy have its greatest sensitivity? The problem of sensitivity applied to inhomogeneities inside multiple scattering media has been addressed in terms of contrast for both fluorescence intensity and fluorescence lifetime.[10] Our paper investigates the sensitivity of fluorescence spectroscopy applied to multiple-scattering media with a uniformly distributed fluorophore.

2. THEORY: THE FREQUENCY-DOMAIN FLUORESCENCE PHOTON DENSITY

2.1 DIFFUSION THEORY

Both emission and excitation photons traveling inside of a highly-scattering medium undergo frequent collisions that give rise to diffusive transport. Diffusion theory, which is a special case of the general formulation of transport theory, has become the standard model used to describe this process.[12,13] The experimental quantity of interest is the photon density, $U(\mathbf{r},t)$ (photons$\times$m^{-3}) where $\mathbf{r}$ represents the distance between the source and the point in space, and t denotes the time. We shall employ diffusion theory to model the propagation of both excitation and emission light signals; throughout this work the subscripts x and m will denote the excitation and the emission, respectively.

Downloaded From: http://proceedings.spiedigitallibrary.org/ on 08/29/2016 Terms of Use: http://spiedigitallibrary.org/ss/termsofuse.aspx

The medium we shall consider may be characterized for our purposes by the optical coefficients μ_{ax} (excitation background absorption coefficient), μ_{am} (emission background absorption coefficient), μ_{sx}' (excitation reduced scattering coefficient), and μ_{sm}' (emission reduced scattering coefficient), all given in cm^{-1}. In addition, we shall uniformly distribute a fluorophore throughout the medium. This fluorophore contributes the *additional* absorptions μ_{afx} and μ_{afm} for the excitation (λ_x) and the emission (λ_m) wavelengths, respectively.

In the framework of diffusion theory in the frequency-domain, the excitation photon density satisfies the familiar equation:

$$\frac{\partial U_x(\mathbf{r},\omega,t)}{\partial t} - vD_x\nabla^2 U_x(\mathbf{r},\omega,t) + v\left[\mu_{ax} + \mu_{afx}\right]U_x(\mathbf{r},\omega,t) = q_x(\mathbf{r},\omega,t), \tag{1}$$

where ω is the angular modulation frequency of the source (not the color of the light), v is the speed of light in water, vD_x is the excitation diffusion coefficient ($cm^2 \times s^{-1}$) defined as $v(3\mu_{sx}')^{-1}$, and $q_x(\mathbf{r},\omega,t)$ is the excitation source term.

Equation (1) may also be expressed for the emission photon density, provided that we use emission-dependent parameters (i.e., D_m, $q_m(\mathbf{r},\omega,t)$ etc.). The main difference between solving the diffusion equation for the excitation and for the emission photon densities lies in the source terms for these photons. We shall now consider the mathematical expressions for these two very different source terms in the frequency-domain approach.

2.2 EXCITATION SOURCE TERM: AN ISOTROPIC POINT SOURCE

In the case of the excitation, the photons are injected into the medium by a light source via an optical fiber or pencil beam. The spatial distribution of the excitation source is assumed to be an isotropic point source. In the frequency-domain approach, such an excitation source has the form:[14]

$$q_x(\mathbf{r},\omega,t) = \delta(\mathbf{r})P(\omega)\exp\left[-i\omega t\right], \tag{2}$$

where $\delta(\mathbf{r})$ is the Dirac delta function, and $P(\omega)$ is the source strength in photons per second.

2.3 EMISSION SOURCE TERM: A DISTRIBUTION OF POINT SOURCES

However, in the case of the emission, there are *many* point sources distributed throughout the medium, since any fluorophore may become an emission point source after absorbing an excitation photon. The strength of a given emission source depends upon four physical factors. First of all, $q_m(\mathbf{r},\omega,t)$ depends upon the excitation photon density at that location (i.e., $U_x(\mathbf{r},\omega,t)$), since a greater density of excitation photons will result in a greater probability of absorption by the fluorophore. Secondly, $q_m(\mathbf{r},\omega,t)$ must scale with the probability of excitation absorption per unit time by the fluorophore, $v\mu_{afx}$. Additionally, we must consider that the emission source radiates into a range of wavelengths. The probability that the fluorophore radiates into a wavelength range $d\lambda$ about λ is given by $\Lambda\varphi_m(\lambda)d\lambda$, where Λ is the fluorescence quantum yield and $\varphi_m(\lambda)$ is the normalized (over all λ) emission

Downloaded From: http://proceedings.spiedigitallibrary.org/ on 08/29/2016 Terms of Use: http://spiedigitallibrary.org/ss/termsofuse.aspx

spectrum of the fluorophore without any scattering. In other words, $\varphi_m(\lambda)$ is the relative emission probability per unit wavelength at λ. Finally, the emission source must reflect the fact that the fluorophore radiates at different times. If we assume a single decay rate, then the fluorophore emits on the average after a time τ (the fluorescence lifetime). After temporal convolution, the emission source term for a single fluorophore becomes:

$$dq_m(\mathbf{r},\omega) = \Lambda v \mu_{afx} \left[\frac{1 + i\omega\tau}{1 + (\omega\tau)^2} \right] U_x(\mathbf{r},\omega) \varphi_m(\lambda_m) d\lambda_m . \tag{3}$$

This expression further assumes negligible photobleaching, and a minimal contribution from fluorescence light that is re-absorbed and eventually re-emitted (i.e., secondary fluorescence). In other words, once an emission photon is absorbed we assume it cannot resurface again.

2.4 THE EMISSION PHOTON DENSITY

The solution to the diffusion equation for the *excitation* photon density, using the source of Eq. (2) takes the well known form[13–15] of $U_x(r,\omega)\exp(-i\omega t)$, where:

$$U_x(r,\omega) = \frac{P(\omega)}{4\pi v D_x} \frac{1}{r} \exp\left[-k_x(\omega) r\right]. \tag{4}$$

In this expression, $k_x(\omega)$ is a complex wave-vector (cm^{-1}) for the photon density wave with the form:

$$k_x^2(\omega) = \frac{\mu_{ax} + \mu_{afx}}{D_x} \left(1 - \frac{i\omega}{v\left\{\mu_{ax} + \mu_{afx}\right\}} \right). \tag{5}$$

This excitation photon density wave travels through the medium, exciting fluorophores in its path, and produces many fluorescence point sources along the way. Each emitting fluorophore creates its own emission photon density of the form of Eq. (4), so that numerous emission photon densities from the individual fluorophores will contribute to the total emission photon density. This fact may be expressed mathematically as a three-dimensional convolution of the emission source (Eq. (3)) with the Green's function for the diffusion equation (i.e., the form of Eq. (4) but with emission parameters). The final result takes the form:[9–11]

$$U_m(r,\omega) = \frac{\Lambda \mu_{afx} \Phi_m P(\omega)}{4\pi v D_x D_m} \left(\frac{1 + \omega\tau}{1 + (\omega\tau)^2} \right) \frac{1}{r} \frac{\exp\left[-k_x(\omega) r\right] - \exp\left[-k_m(\omega) r\right]}{k_m^2(\omega) - k_x^2(\omega)}. \tag{6}$$

The factor Φ_m is a factor that contains the experimental detection system's relative spectral response, as well as the fluorophore emission efficiency $\varphi_m(\lambda_m)$. Φ_m may be determined experimentally. The concentration of the fluorophore (i.e., μ_{afx}) is contained within the k_x. Only in the limit $\mu_{afx} << \mu_{ax}$ is $U_m(r,\omega)$ linear with μ_{afx}.

Downloaded From: http://proceedings.spiedigitallibrary.org/ on 08/29/2016 Terms of Use: http://spiedigitallibrary.org/ss/termsofuse.aspx

3. EXPERIMENTAL METHODS

3.1 EXPERIMENTAL APPARATUS: A TOUR OF THE FREQUENCY-DOMAIN SPECTROMETER

Figure 1 outlines the major components of our frequency-domain spectrometer. The excitation source is a mode-locked frequency-doubled Nd:YAG laser (Coherent, Palo Alto, CA) pulsed at 76.2 MHz. A 10X optical objective focuses this 532 nm beam into a bifurcated solid plastic optical fiber (1.5 mm core diameter). A lens focuses light from the smaller leg of the fiber (1 mm core diameter) onto a reference photomultiplier tube (PMT; Hamamatsu, model R928). The signal from this reference PMT corrects for drifts in the laser intensity and provides a phase reference. The main leg of the bifurcated fiber (1.5 mm core diameter), known as the source fiber, carries the excitation light into the sample medium. The container for the liquid sample is an 8 L cylindrical tank with a diameter of 30 cm and a height of 14 cm. A glass fiber optic bundle (Oriel, Stratford, CT; 3.2 mm bundle diameter, 0.56 numerical aperture), known as the sample fiber, collects photons from within the sample. Both source and sample fibers are placed in the tank's center 6 cm below the surface of the sample medium, effectively simulating an infinite medium geometry. A computer-controlled 3D position scanner positions the sample fiber in the medium in 1.00±.01 mm steps.

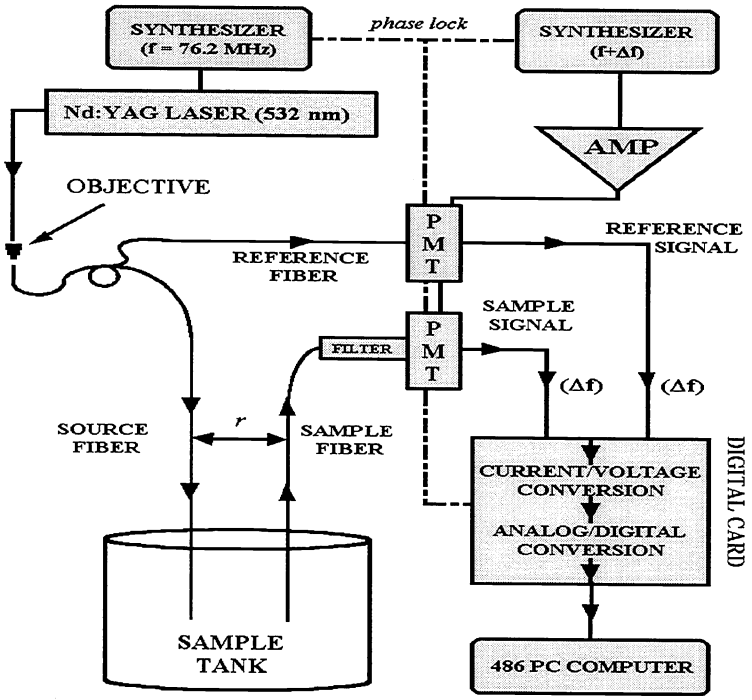

Figure 1 - *Experimental Apparatus.* A Nd:YAG laser modulated at 76.2 MHz provides a 532 nm laser beam that is focused into a bifurcated optical fiber by an optical objective. One leg of this fiber directs light to a reference PMT to correct for laser drifts and to provide a reference for the phase. The other leg of the bifurcated fiber (the source fiber) injects light into the sample medium. Another fiber (the sample fiber) collects light from inside the medium. Both source and sample fibers are placed inside the 8 L sample volume to form an infinite medium geometry. Although not shown, the sample fiber may be moved by a computer-controlled 3D positioning device. The sample fiber sends the collected light to a filter box, where an optical interference filter is placed. After the filter, the light is focused onto a sample PMT. Both PMT's are driven by an amplified synthesizer signal modulated at 76.2004 MHz. The sample and reference signals are independently cross-correlated down to 400 Hz, and sent to a data acquisition card located inside a 486 PC computer. The card converts the current to a voltage and then digitizes the voltage. Software records the sample and reference *DC* counts, *AC* sample counts, and the phase. All components of this instrument are phase locked, as indicated by the dotted lines in the figure. Also not shown is the mixing plate used to keep the particles in solution.

The sample fiber directs the light signal from the phantom to a filter box that holds optical filters in a reproducible manner. A fluorescence interference filter centered at 580 nm (Corion; XM-585-F; 10 nm FWHM) passes the emission light. After the filter, another lens focuses the light onto a sample PMT. A synthesizer (Marconi Instruments, Allendale, NJ; model 2022A) provides a signal modulated at 76.2004 MHz that is amplified (ENI, Rochester, NY) and then used to modulate both reference and sample PMT's as described by Gratton and Limkeman.[16] The modulated PMT currents are beat with the 76.2 MHz laser modulation frequency. The resulting 400 Hz heterodyned signals (reference and sample) are then processed by a 12 bit digital acquisition

Downloaded From: http://proceedings.spiedigitallibrary.org/ on 08/29/2016 Terms of Use: http://spiedigitallibrary.org/ss/termsofuse.aspx

card (ISS, Inc., Champaign, IL), which converts the PMT currents into voltages, and then digitizes the voltages.[17] Software (ISS, Inc.) run on a 486 PC computer records the phase, *DC* intensity (sample and reference), and the sample *AC* amplitude. All components of the apparatus are phase locked, as indicated by the dotted lines in Fig. 1.

3.2 SAMPLE: A MULTIPLE SCATTERING PHANTOM WITH A UNIFORMLY DISTRIBUTED FLUOROPHORE

The tissue-like sample phantom consisted of an aqueous suspension of titanium-dioxide particles from white paint, mixed with black-india ink. Continuous mixing ensured that the particles remained suspended in the water. This part of the phantom will be referred to as the 'background', since it does not fluoresce within our wavelength region of interest. The frequency-domain spectrometer was needed to measure the phantom's background optical coefficients. For this measurement, we employed a multiple-distance, single-modulation frequency protocol.[18] The measured optical coefficients are recorded below in Table I. These particular values were chosen to reflect the optical properties of tissue exposed to near-IR light. In order to measure the phantom's background properties at 580 nm, a 580 nm beam from a Nd:YAG pumped rhodamine-6G dye laser (Coherent) excited the sample, and the signal was detected after passing through the 580 nm interference filter.

COEFFICIENT	532 nm	580 nm
BACKGROUND ABSORPTION (cm^{-1})	(μ_{ax}) 0.0877 ± 0.0004	(μ_{am}) 0.0817 ± 0.0004
BACKGROUND REDUCED SCATTERING (cm^{-1})	(μ_{sx}') 12.9 ± 0.1	(μ_{sm}') 12.0 ± 0.1
FLUOROPHORE EXTINCTION ($M^{-1} \times cm^{-1}$)	(ε_{532}) 4.64×10^4	(ε_{580}) 1.33×10^4

Table I - *Optical properties of the phantom at the excitation (532 nm) and the emission (580 nm) wavelengths.* The background absorption and reduced scattering were measured using the frequency-domain spectrometer as described above. Note that of these four coefficients are not related to the fluorescence properties of the rhodamine. The extinction coefficients were measured using a commercial spectrophotometer along with a published value of the extinction coefficient at the absorption spectrum peak (554 nm). The extinction coefficients are presented in base 10. The symbol for each coefficient is provided in parentheses for convenience.

The fluorophore in the phantom was laser-grade rhodamine B (Eastman Kodak, Rochester, NY). Rhodamine B in water has a lifetime of 1.5 ns and a quantum yield of 0.31. Given that rhodamine B undergoes single exponential decay and does not photobleach easily, it is compatible with our assumptions for Eq. (6).[19] The rhodamine does not interact appreciably with the titanium-dioxide particles. The non-scattering absorption spectrum of this fluorophore was obtained from a commercial spectrophotometer, which provided the extinction coefficient ratios. We were able to determine the extinction coefficient at each wavelength of interest by using a published vale for the extinction coefficient at the absorption maximum, namely $\varepsilon_{554} = 10.3 \times 10^4\ M^{-1}\ cm^{-1}$.[19] Concentrations in the spectrophotometer were kept below 1 μM, ensuring that no rhodamine dimers formed.

3.3 EXPERIMENTAL PROTOCOL

Once the background optical properties of the phantom had been determined with the frequency-domain spectrometer, we then added the fluorophore. The excitation wavelength was always $\lambda_x = 532$ nm. The experiment followed two basic steps. First, we added rhodamine B from our aqueous stock solution (179 μM) to the phantom with a pipette. After thoroughly mixing the solution, we then measured the *DC* fluorescence intensity (also referred

Downloaded From: http://proceedings.spiedigitallibrary.org/ on 08/29/2016 Terms of Use: http://spiedigitallibrary.org/ss/termsofuse.aspx

to as emission) over a range of source-detector separations (also referred to as *r*), namely 1.0 to 3.4 cm, in 4 mm steps, using the 580 nm interference filter. The *DC* reference channel was also recorded. This multiple-distance scan was repeated three times, resulting in three measurements for each source-detector separation at each measured rhodamine concentration in the phantom. We also performed a measurement on the *background* phantom (i.e., no fluorophore) excited at 532 nm using the emission filter to measure the amount of excitation light leaking through the 580 nm interference filter. This excitation background was subtracted from the measured *DC* fluorescence intensity.

4. EXPERIMENTAL RESULTS

Table II presents a portion of the measured data. The first column provides the amount of 179 μM rhodamine stock solution added to the 8 L phantom in units of volume (μL). The next column translates this amount into a concentration (nM) within the phantom. The volumes are accurate to within 1% since they were administered with a calibrated pipette. The concentrations suffer from an error of approximately 7% due to the uncertainty in measuring out the 8 L phantom volume. For our purposes this will not be a problem, since the systematic error essentially becomes a scale factor.

The next three columns display the *DC* fluorescence intensity detected at 580 nm, measured at the source-detector separations of 1.8, 2.6, and 3.0 cm. Each measured intensity had passed through the 580 nm interference filter. There are three important experimental points to be noted about the acquisition of these values:

1) Some excitation light still managed to leak through the 580 nm interference filter. These background excitation signals have *already* been subtracted from the *DC* intensity values presented in Table II, as we mentioned previously. Thus, we are assured that these intensity data represent purely emission signals.
2) Each signal has been *scaled* to the first measurement via the *DC* reference channel. This sample channel scaling accounts for drifts in the laser.
3) The listed uncertainties are the *standard deviations* from the three independent multiple-distance scans. All of the uncertainties reflect the standard deviations of both the sample and reference channels, taking care to properly combine them since these errors are not independent. The errors in measuring the background subtraction have also been incorporated.

Since the counts listed are only proportional to the photon density, they are arbitrary. Nevertheless, these count values for our purposes may be used with absolute meaning. As has been previously demonstrated, we may measure the spectral response of the detector, which enables us to find the absolute quantum yield of the fluorophore.[11]

Downloaded From: http://proceedings.spiedigitallibrary.org/ on 08/29/2016 Terms of Use: http://spiedigitallibrary.org/ss/termsofuse.aspx

RHODAMINE		*DC* FLUORESCENCE INTENSITY AT 580 nm		
[μL]	[nM]	$r = 1.8$ cm	$r = 2.6$ cm	$r = 3.0$ cm
40	0.894	6.14 ± 0.02	1.67 ± 0.05	0.89 ± 0.12
2400	53.7	335.4 ± 2.5	81.3 ± 2.0	39.3 ± 1.4
2520	56.4	353.9 ± 3.4	83.00 ± 0.48	40.75 ± 0.03
2600	58.2	366.4 ± 7.7	86.42 ± 0.14	41.69 ± 0.49
2640	59.1	375.7 ± 3.8	88.55 ± 0.58	42.7 ± 0.3
16000	357	1751 ± 44	358.9 ± 0.8	160.8 ± 1.2
16160	361	1784 ± 27	368.7 ± 4.5	168.0 ± 2.2
16800	375	1882 ± 26	384.8 ± 2.7	176.2 ± 0.6

Table II - DC *fluorescence intensity in the phantom with a fluorophore measured at 580 nm.* The first column reports the amount of stock rhodamine solution added to the phantom in terms of volume (μL). The next column converts the volume into a concentration (nM) in the phantom. The next three columns report the measured *DC* fluorescence intensity detected through the 580 nm interference filter at source-detector separations of 1.8, 2.6, and 3.0 cm. These data were scaled with the *DC* reference channel to filter out drifts in the excitation laser intensity. Each value represents the average of three measurements. The uncertainties are the standard deviations, taking into account the dependent nature of the errors in both sample and reference channels. Since some excitation light still passed through the 580 nm interference filter, a small excitation background subtraction was taken from these data.

5. DISCUSSION

5.1 MEASURING NM FLUOROPHORE CONCENTRATIONS

One of the most striking features of the data is that measurable signals emerge from rhodamine concentrations in the phantom as little as 1 nM. For example, we collected 25.36 ± 0.25 *DC* fluorescence counts at the closest source-detector separation of 1 cm from a phantom with a rhodamine concentration of only 0.894 nM. This measurement is even more striking when we consider that for rhodamine B in water, a concentration of 1 nM creates a μ_{afx} of only 0.0001 cm^{-1}. Detecting the change in the excitation light emerging from such a small change in absorption via differential absorption spectroscopy is impossible with our instrument, since the change falls within the error of the measurement. Also, changes in the excitation intensity were concealed by the noise of the measurement. Therefore, we have evidence that in the diffusion regime, nM fluorophore concentrations are measurable, even if concealed behind a substantial background absorption.

5.2 HOW FLUORESCENCE INTENSITY CHANGES WITH REDUCED SCATTERING

The detection of such large fluorescence signals from such small fluorophore concentrations is plausible if we consider that the multiple-scattering medium *increases* the path length of the excitation light. In a standard cuvette for a commercial spectrophotometer (where minimal scattering is present), the path length is typically 1 cm. In our example (at 0.894 nM) the excitation path length is on the order of 10 cm even though the source-detector separation is only 1 cm. As the reduced scattering increases, more and more fluorophores will be able to contribute

Downloaded From: http://proceedings.spiedigitallibrary.org/ on 08/29/2016 Terms of Use: http://spiedigitallibrary.org/ss/termsofuse.aspx

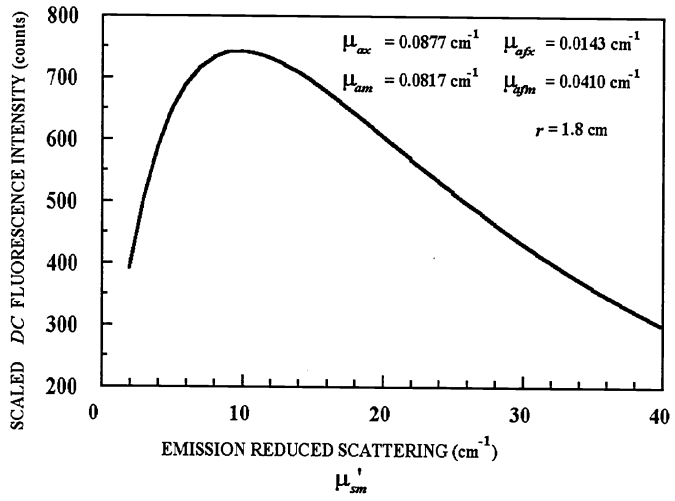

Figure 2 - DC *fluorescence intensity Vs. emission reduced scattering coefficient.* This plot is a calculation using Eq. (6) with the coefficients of Table I. The reduced scattering of the excitation was changed along with that of the emission according to an experimentally determined ratio as given in the text. The fluorophore concentration was 134 nM, and the source-detector separation was 1.8 cm. There is a clear peak in the *DC* fluorescence intensity near $\mu_{sm}' \sim 10$ cm^{-1}. The location of the peak changes with fluorophore concentration, but it remains close to 10 cm^{-1} for these data.

to the resulting emission signal because the excitation photons travel along longer path lengths in the phantom. However, at some level the scattering will become so great that the excitation and emission photon densities will be severely attenuated.

Figure 2 demonstrates this balance. Using Eq. (6), this plot is a calculation of the *DC* fluorescence intensity as a function of the emission reduced scattering coefficient, μ_{sm}'. The scale of the *DC* emission values is the same scale as that of the measured data. Both μ_{sx}' and μ_{sm}' were changed together for this calculation according to an experimentally determined reduced scattering vs. wavelength derivative (-0.019 cm$^{-1}\times$nm^{-1}). The rhodamine concentration in the phantom was 134 nM, and the source-detector separation was 1.8 cm. All other values, such as the absorption and extinction coefficients, were taken from Table I. The absorption due to the fluorophore (calculated using the extinction coefficients in Table I) is given in the figure. Although the peak of the emission signal varies for different fluorophore concentrations, the emission maximum stays relatively close to $\mu_{sm}' \sim 10$ cm^{-1}. This value of the reduced scattering is of the same order as those found in tissues.

5.3 SMALL CONCENTRATION CHANGES EXPERIMENTALLY RESOLVABLE WITH FLUORESCENCE INTENSITY

How reliably may we use the *DC* fluorescence intensity to resolve two similar, yet different, concentrations? By the term 'resolve' we imply that the two signals, including errors, do not overlap; they are experimentally distinguishable. In our measurements, we could consistently experimentally resolve between changes in the *DC* fluorescence intensity with concentration changes of about 5 % (56.4 to 59.1 nM). Smaller concentration changes from 56.4 to 58.2 nM (3.2 %) were also resolvable for all source-detector separation of 1.8 cm or greater. We were not able to consistently resolve between signals with changes of 1.5 % in rhodamine concentration, but the failures were again at the closest distances. This concentration change is on the order of 1 nM at 54 nM. Note that even a 10 nM change would be difficult to resolve if we used only the excitation intensity, yet here a 10 nM change is easily resolvable if we use the fluorescence intensity.

The same general pattern exists in the 357 nM range. Changes of 1 % (357 to 361 nM) in rhodamine concentration were resolvable for the larger source-detector separations, whereas changes in the neighborhood of 5 % were always resolvable (i.e., 357 to 375 nM). A change of 5% at this concentration results in a 18 nM change, which translates into a μ_{afx} of 0.0019 cm^{-1}. This value is still within the noise region for the determination of

Downloaded From: http://proceedings.spiedigitallibrary.org/ on 08/29/2016 Terms of Use: http://spiedigitallibrary.org/ss/termsofuse.aspx

absorption coefficients with our system (the *total* absorption here is $0.130 \pm 0.005\ cm^{-1}$). Of course, these sensitivity values are dependent upon the stability of the excitation source. Using sources with improved stability, such as laser diodes, would further improve these resolvability limits. In summary, the greatest success in resolvability (detecting approximately 1% changes in concentration) occurred at the *longer* source detector separations (3.0 and 3.4 cm) when enough signal was present. The worst success in resolvability occurred at the shorter distances (1.0 and 1.4 cm).

5.4 FLUORESCENCE SENSITIVITY DEPENDS UPON SOURCE-DETECTOR SEPARATION AND CONCENTRATION

Figure 3 presents the *DC* fluorescence intensity calculated as a function of rhodamine concentration. The rhodamine concentrations have also been given in terms of μ_{afx}. The plot reflects the predictions of Eq. (6) with the data of Table I, using source-detector separations of 1.0, 2.6, and 3.4 cm. The absorption coefficients due to the fluorophore (μ_{afx} and μ_{afm}) were calculated using the extinction coefficients presented in Table I. For the sake of comparison, all three curves have been independently normalized. The maxima of these curves, using the same scale as in Fig. 2, occur at 12600, 314, and 59.7 counts for the source-detector separations of 1.0, 2.6, and 3.4 cm, respectively.

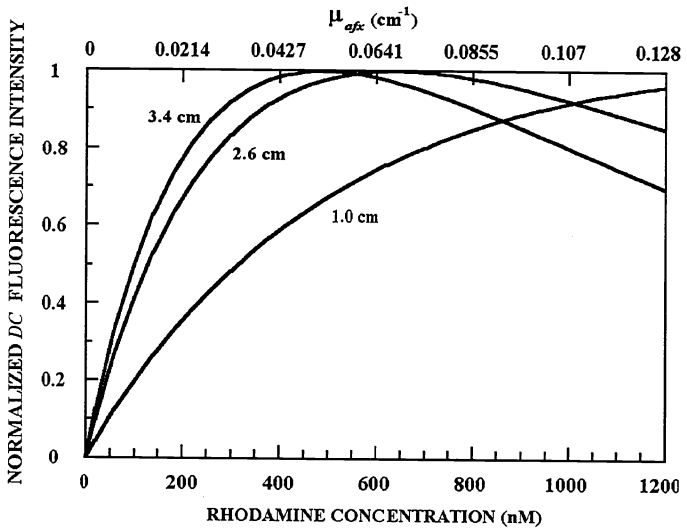

Figure 3 - *Normalized DC fluorescence intensity Vs. rhodamine concentration.* Eq. (6) was used to calculate the fluorescence intensity as a function of rhodamine concentration for three different source-detector separations. Data for the plot was taken from Table I. Note that the concentration where the emission maximum occurs decreases significantly with increasing source-detector separation.

The sensitivity, defined as the ability to resolve, is related to the slope of these curves. The sensitivities of these curves may be compared assuming an equal error in each case. We see that in the 50 nM region, relative changes in the *DC* fluorescence intensity are more dramatic for the larger source-detector separations. This is consistent with our observations; we were able to resolve smaller changes in sample concentration with larger source-detector separations, as mentioned above. In the region of 54 nM, the plots are approximately linear, and our best sensitivity results. In the region of 360 nM, we see that the fluorescence begins to level off, and hence some sensitivity is lost. Eventually the fluorescence reaches a maximum, the slope approaches zero, and the sensitivity vanishes. An important observation is that the fluorophore concentration at this maximum *decreases sharply* with an increase in source-detector separation. Continuing onward with increasing fluorophore concentration, we see that the *DC* fluorescence intensity actually begins to decrease, an effect which has been noted previously.[9] If we go to higher fluorophore concentrations, the sensitivity begins to improve since the magnitude of the slope begins to increase.

Downloaded From: http://proceedings.spiedigitallibrary.org/ on 08/29/2016 Terms of Use: http://spiedigitallibrary.org/ss/termsofuse.aspx

The location of the fluorophore concentration where the slope vanishes is a balance between the conversion rate of excitation to emission photons and the absorption rate of the emission photons. When relatively few fluorophores are present, an increase in the number of fluorophores will increase the excitation absorption rate, and hence increase the rate of emission photon generation. However, changing the fluorophore concentration will also change the absorption of the emission intensity (see Table I).

It is clear from the above measurements that the sensitivity of fluorescence spectroscopy greatly exceeds that of normal absorption spectroscopy in the limit of small chromophore concentrations. However, this advantage is not enjoyed over all chromophore concentrations. This may be seen with a calculation comparing the signal-to-noise ratios for changes in the detected signal for both emission and excitation photon densities. For the data presented here, small fractional changes in the concentration will be easier to detect with changes in the emission intensity as compared to changes in the excitation intensity for concentrations below approximately 600 nM and 180 nM for source detector separations of 1.0 and 3.4 cm, respectively.[11]

6. CONCLUSIONS

From within the diffusion regime, we were able to detect measurable *DC* fluorescence intensities from 1 nM concentrations of rhodamine uniformly distributed inside of a realistic absorbing and scattering tissue-like phantom. The increased path length of the excitation photons provided by the multiple scattering phantom permits these relatively low concentrations of fluorophores to build up into a detectable emission photon density. Changes in concentration as small as approximately 1% were resolved using the *DC* fluorescence intensity, although this level of resolvability was found only for the longer source-detector separations. We could resolve at least 5% changes in fluorophore concentration for every source-detector separation (1.0 to 3.4 cm) examined. A more stable excitation source should permit better resolution. Using a frequency-domain fluorescence photon migration model, we were able to see that the fluorescence sensitivity experiences pronounced changes as functions of fluorophore concentration and source-detector separation. The concentration where the fluorescence peaks, and subsequently where the sensitivity is the poorest, decreases with increasing source-detector separation. This variation in source-detector separation may allow for precise concentration determination with a multiple-distance protocol. We also used the fluorescence photon migration model to demonstrate that the emission signal peaks at reduced scattering values in the range of those encountered in tissues.

7. ACKNOWLEDGMENTS

This work performed at the Laboratory for Fluorescence Dynamics, and was supported by NIH grants RR03155, CA57032 and by a Whitaker-NIH grant RR10966.

8. REFERENCES

1 *Biomedical Optical Spectroscopy and Diagnostics*, D. Benaron and E. Sevick-Muraca, eds., 1996 OSA Technical Digest (Optical Society of America, Washington D.C., 1996).

2 D. T. Delpy, M. Cope, P. van der Zee, S. Arridge, S. Wray, and J. Wyatt, "Estimation of optical pathlength

Downloaded From: http://proceedings.spiedigitallibrary.org/ on 08/29/2016 Terms of Use: http://spiedigitallibrary.org/ss/termsofuse.aspx

through tissue from direct time of flight measurement," *Phys. Med. Biol.* **33**, 1433-1442 (1988).

3 H. Miyake, S. Nioka, A. Zaman, D. S. Smith, and B. Chance, "The detection of cytochrome oxidase heme iron and copper absorption in the blood-perfused and blood-free brain in normoxia and hypoxia," *Anal. Biochem.* **192**, 149-155 (1991).

4 R. Richards-Kortum, R. P. Rava, M. Fitzmaurice, L. L. Tong, N. B. Ratliff, J. R. Kramer, and M. S. Feld, "A one layer model of laser-induced fluorescence for diagnosis of disease in human tissue: applications to atherosclerosis," *IEEE Trans. Biomed. Eng.* **36**, 1222-1232 (1989).

5 J. M. Devoisselle, S. Soulie, S. Mordon and H. Maillols, "Fluorescent characteristics and pharmacokinetic profiles of the fluorescent probe BCECF in various tissues: the role of blood content," *Photochem. Photobiol.* **64**, 906-910 (1996).

6 H. Szmacinski and J. R. Lakowicz, "Lifetime-based sensing," *Topics in Fluorescence Spectroscopy: Volume 4,* ed. by J. R. Lakowicz, (Plenum, New York, 1994).

7 J. Wu, M. S. Feld, and R. P. Rava, "Analytical model for extracting intrinsic fluorescence in turbid media," *Appl. Opt.* **32**, 3585-3595 (1993).

8 E. M. Sevick-Muraca and C. L. Burch, "Origin of phosphorescence signals reemitted from tissues," *Opt. Lett.* **19**, 1928-1930 (1994).

9 M. S. Patterson and B. W. Pogue, "Mathematical model for time-resolved and frequency-domain fluorescence spectroscopy in biological tissues," *Appl. Opt.* **33**, 1963-1974 (1994).

10 X.D. Li, M. A. O'Leary, D. A. Boas, B. Chance, and A. G. Yodh, "Fluorescent diffuse photon density waves in homogeneous and heterogeneous turbid media: Analytic solutions and applications," *Appl. Opt.* **35**, 3746-3758 (1996).

11 A. E. Cerussi, J. S. Maier, S. Fantini, M. A. Franceschini, W. W. Mantulin, and E. Gratton, "Experimental verification of a theory for the time-resolved fluorescence spectroscopy of thick tissues," *Appl. Opt.* **36**, 116-124 (1997).

12 J. J. Duderstadt and L. J. Hamilton, *Nuclear Reactor Analysis* (John Wiley & Sons, New York, 1976).

13 M. S. Patterson, B. Chance, and B. C. Wilson, "Time-resolved reflectance and transmittance for the non-invasive measurement of tissue optical properties," *Appl. Opt.* **28**, 2331-2336 (1989).

14 J. B. Fishkin and E. Gratton, "Propagation of photon-density waves in strongly scattering media containing an absorbing semi-infinite plane bounded by a straight edge," *J. Opt. Soc. Am. A.* **10**, 127-140 (1993).

15 S. R. Arridge, M. Cope, and D. T. Delpy, "Theoretical basis for the determination of optical path lengths in tissue: temporal and frequency analysis," *Phys. Med. Biol.* **37**, 1537-1560 (1992).

16 E. Gratton and M. Limkeman, "A continuously variable frequency cross-correlation phase fluorometer with picosecond resolution," *Biophys. J.* **44**, 315-324 (1983).

17 B. Feddersen, D. W. Piston, and E. Gratton, "Digital parallel acquisition in frequency-domain fluorimetry," *Rev. Sci. Instr.* **60**, 2929-2936 (1989).

18 S. Fantini, M. A. Franceschini, J. B. Fishkin, B. Barbieri, and E. Gratton, "Quantitative determination of the absorption spectra of chromophores in strongly scattering media: a light-emitting-diode based technique," *Appl. Opt.* **33**, 5204-5213 (1994).

19 F. López Arbeloa, T. López Arbeloa, M. J. Tapia Estévez, and I. López Arbeloa, "Photophysics of rhodamines: molecular structure and solvent effects," *J. Phys. Chem.* **95**, 2203-2208 (1991).

For further information:

corresponding author:	A. E. Cerussi
e-mail	cerussi@uiuc.edu
phone	(217)244-5620
fax	(217)244-7187
www	http://www.physics.uiuc.edu/groups/fluorescence

Downloaded From: http://proceedings.spiedigitallibrary.org/ on 08/29/2016 Terms of Use: http://spiedigitallibrary.org/ss/termsofuse.aspx